Unidirectional Excitation of Radiative-Loss-Free Surface Plasmon Polaritons in PT-Symmetric Systems

Wei Wang, Lu-Qi Wang, Rui-Dong Xue, Hao-Ling Chen, Rui-Peng Guo, Yongmin Liu, and Jing Chen

Phys. Rev. Lett. **119**, 077401 — Published 16 August 2017

DOI: 10.1103/PhysRevLett.119.077401

Unidirectional Excitation of Radiative-Loss-Free Surface Plasmon Polaritons in Parity-Time Symmetric Systems

Wei Wang[1, 2], Lu-Qi Wang[1], Rui-Dong Xue[1], Hao-Ling Chen[1], Rui-Peng Guo[1], Yongmin Liu[2, 3], and Jing Chen[1, 4]

[1] *School of Physics, Nankai University, Tianjin 300071, P. R. China*

[2] *Department of Mechanical and Industrial Engineering and Department of Electrical and Computer Engineering, Northeastern University, Boston, Massachusetts 02115, USA*

[3] *y.liu@northeastern.edu*

[4] *jchen4@nankai.edu.cn*

ABSTRACT: We investigate the excitation and propagation of surface plasmon polaritons (SPPs) at a geometrically flat metal-dielectric interface with a parity-time symmetric modulation on the permittivity ε(x) of the dielectric medium. We show that two striking effects can be simultaneously achieved thanks to the nonreciprocal nature of the Bloch modes in the system. Firstly, SPPs can be unidirectionally excited when light is normally incident on the interface. Secondly, the backscattering of SPPs into the far field is suppressed, producing a radiative-loss-free effect on the unidirectional SPPs. As a result, the life time and propagation distance of SPPs can be significantly improved. These results show that parity-time symmetry can be employed as a new approach to designing transformative nanoscale optical devices, such as low-loss plasmonic routers and isolators for efficient optical computation, communication and information processing.

PACS: (73.20.Mf) Surface plasmons; (05.30.Rt) Quantum phase transitions; (42.25.Fx) Optical diffraction.

For a long time, absorption characterized by the imaginary component (ε_i) of the dielectric constant ($\varepsilon = \varepsilon_r + i\varepsilon_i$) was believed to play an undesirable role in optics, and should be mitigated and even eliminated. However, with the novel concepts of non-Hermitianal Hamiltonian [1-5] and parity-time (*PT*) symmetry [6-20], recently there have been increasing interests in manipulating the dynamics of optical waves via controlling the distribution of ε_i. Through engineering the spatial variation of gain ($\varepsilon_i < 0$) and loss ($\varepsilon_i > 0$), various attractive phenomena and important applications have been proposed and demonstrated. For example, Guo *et al.* [6] reported loss induced optical transparency in specially designed pseudo-Hermitian guiding potentials. Longhi [8] and Chong *et al.* [9] discussed the realization of a coherent perfect absorber as the time-reversed counterpart of a laser. Lin *et al.* [10] and Feng *et al.* [11] studied the unidirectional invisibility and reflectionless waveguide based on *PT* symmetry. The conservation relations and anisotropic transmission resonances in one-dimensional *PT*-symmetric photonic heterostructures were analyzed by Ge *et al.* [13]. In Ref. [14], Fleury *et al.* introduced a new mechanism to realize negative refraction and planar focusing using a pair of *PT* symmetric metasurfaces. Peng *et al.* [15] showed how to turn losses into gain by steering the parameters of a system to the vicinity of an exceptional point (EP). *PT* symmetry in other metamaterials [16-19] and its nonlinear optical effects [20] have also been studied by various groups.

Surface optical waves, such as surface plasmon polaritons (SPPs), have attracted much attention in the past decades because of its quasi-2D and sub-wavelength nature [21, 22]. An efficient means to manipulate SPPs, including directional excitation and a longer propagation distance (or equivalently a longer lifetime), is always desired because it determines the figure of merit of SPP-related applications [23-30]. In this Letter we show that by using a *PT* symmetric modulation on the permittivity of the dielectric medium adjacent to a metal, we can realize unique features of SPPs at a geometrically flat dielectric-metal interface. We demonstrate that with a properly designed spatial distribution of ε_r and ε_i in the spirit of *PT* symmetry, a unidirectional excitation of SPPs can be achieved even under the condition of normal incidence. Furthermore, the *PT* symmetric configuration breaks the reciprocal back-and-forth mutual coupling between the propagating bulk wave and SPPs, and produces a radiative-loss-free effect on the unidirectional generated SPPs with substantially improved life time. The underlying mechanism of these novel effects is closely related to an EP of the *PT* symmetric modulation, which is not due to a square root singularity and fundamentally different from previous work [2, 4, 31]. Such unidirectional and radiative-loss-free SPPs can be utilized for many potential applications.

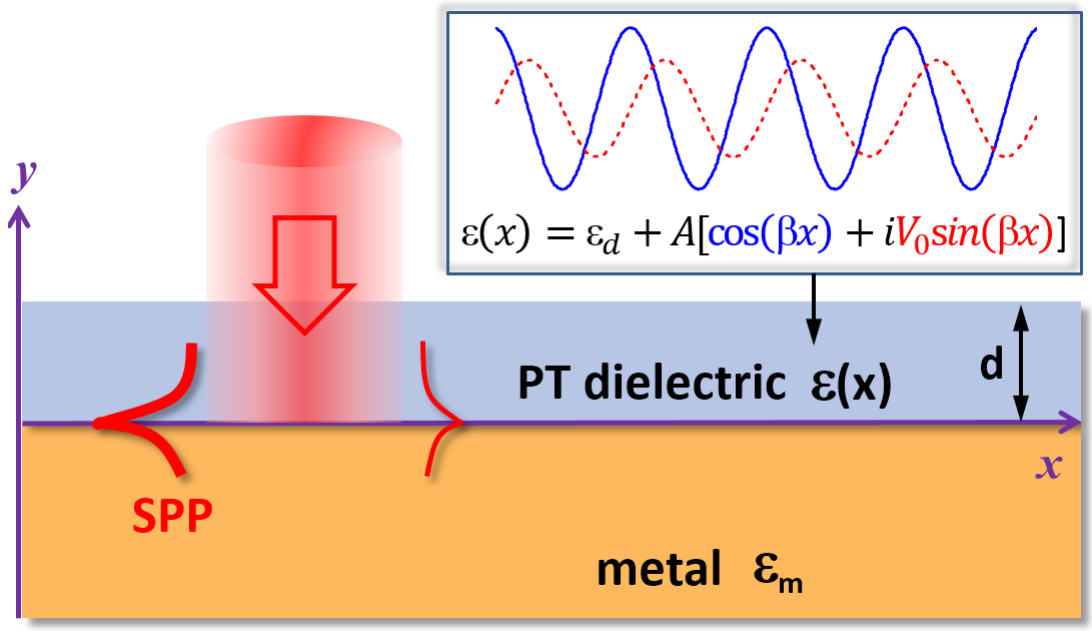

FIG. 1. Schematic of the proposed structure. A *PT* dielectric layer with a thickness d and dielectric constant $\varepsilon(x) = \varepsilon_d + A(\cos\beta x + iV_0\sin\beta x)$ is placed above a metal slab with $\varepsilon_m < 0$. An optical beam is normally incident on the structure, exciting asymmetric or even unidirectional SPPs.

Figure 1 shows a schematic of the proposed structure under investigation. A metal slab with a dielectric constant of $\varepsilon_m<0$ occupies the space below y=0. Above the metal we introduce a dielectric layer of thickness d. The dielectric layer supports a *PT* symmetric distribution of $\varepsilon(x)$ in the form of [5, 32, 33]

$$\varepsilon(x) = \varepsilon_d + A(\cos\beta x + iV_0\sin\beta x). \quad (1)$$

Parameter ε_d represents the background dielectric constant, and the modulation strength A is much smaller than ε_d. The real part of $\varepsilon(x)$ is symmetric with respect to x=0, while the imaginary part is anti-symmetrically distributed.

The interface at y=0 is geometrically smooth. When the *PT* symmetric modulation is absent (*i.e.*, A=0), the normally incident beam simply oscillates inside the layer and gets reflected. When A is not zero, the periodic modulation of the permittivity, that is, $\Delta\varepsilon(x)=A[\cos(\beta x) + iV_0\sin(\beta x)]$, could provide the required phase matching condition to excite SPPs. By using COMSOL Multiphysics we simulate the interaction of a normally incident beam with the structure. Dielectric constants considered in the simulation are $\varepsilon_m = -100+4i$ [34] and $\varepsilon_d = 6$. The thickness d of the dielectric layer is $0.29\lambda_0$, and the beam width of incidence is $5\lambda_0$, where λ_0 is the wavelength in vacuum. Parameter β equals the real part of the wavevector of the

corresponding SPP mode,

$$\square = k_0\sqrt{\frac{\varepsilon_d\varepsilon_m}{\varepsilon_d+\varepsilon_m}} \quad (2)$$

where $k_0 = 2\pi/\lambda_0 = \omega_0/c$. Note that for a finite dielectric cladding layer the wavevector of SPPs may be different from Eq. (2), and an analytical formula can be found from [35]. However, the expression given by Eq. (2) provides an accurate estimation of the necessary phase-matching wavevector when the permittivity modulation $\Delta\varepsilon(x)$ is small, and ensures a resonant excitation of SPPs at normal incidence.

Figure 2(a) shows the transverse magnetic field component (H_z) when V_0=0. In this case, the dielectric constant $\varepsilon(x)$ is real everywhere, and a standard dielectric grating is realized. We can see that SPPs are equally excited on both sides of the incident beam, in agreement with the theory on the scattering of optical wave by subwavelength gratings [21, 22]. However, the characteristic of excited SPPs is distinctly different when *PT* symmetry is introduced into the dielectric layer. Figure 2(b) shows the result when V_0=0.5. We can see that by increasing the value of V_0, *i.e.,* the magnitude of the modulation on ε_i, the excitation of SPPs along the forward and backward directions becomes unequal. For the result shown in Fig. 2(b), SPPs are much more efficiently excited towards the left side of the incident beam. The degree of unequal SPP generation reaches its extreme scenario at the critical point of V_0=1, with which the excitation of SPPs on the right side of incidence is completely suppressed [see Fig. 2(c)]. Now a unidirectional excitation of SPPs is obtained. Note that the propagation direction of generated SPPs can be tuned by changing the sign of V_0. To be more explicitly, when V_0= −1 SPPs are generated only on the right side of incidence.

The field distribution and their oscillation period agree well with the features of SPPs. From Figs. 2(d) and (e) we can see that the field is enhanced at the dielectric-metal interface, and the period of oscillation is given by $\beta \sim 2.526k_0$, in very good agreement with Eq. (2). In addition to the asymmetric excitation of SPPs on opposite sides of incidence when V_0 increases, we also notice that the efficiency of SPP excitation is dependent on V_0. Figure 3 shows the distributions of the envelop of H_z at the metal-dielectric interface for V_0 = 0, 0.5, and 1, respectively. When V_0 = 1 the excitation of SPPs on the left side of incidence is obviously greater than that on the right side when V_0=0 or 0.5.

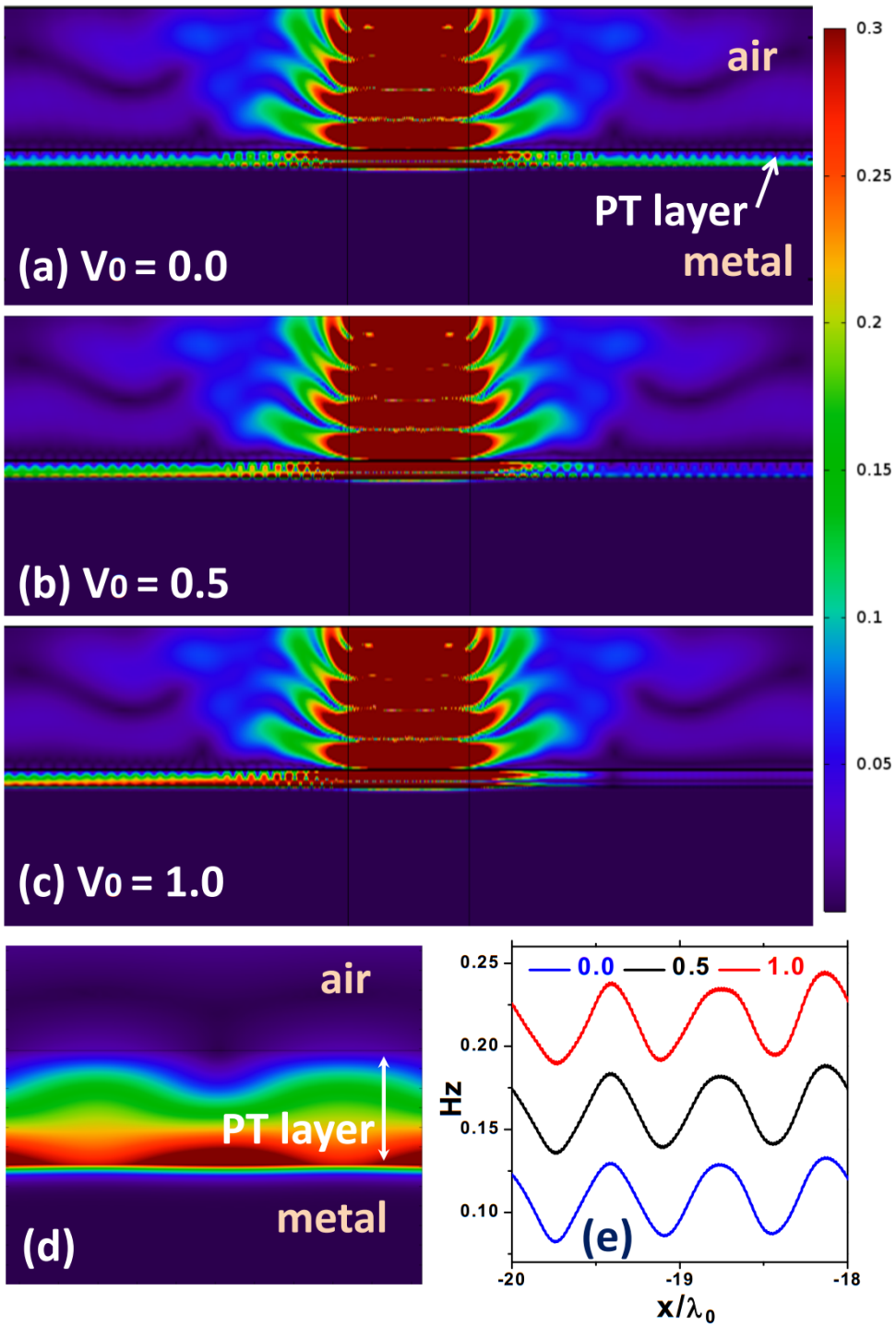

FIG. 2. Simulation results on the two-dimensional distribution of H_z component for normal incidence when (a) V_0=0, (b) V_0=0.5, and (c) V_0=1, respectively. When V_0=0, SPPs are equally excited on both sides of the incident beam. When V_0=1, SPPs are predominantly excited towards the left side. Plot (d) is a zoomed in picture of the field distribution in one period, and (e) shows the distribution of H_z amplitude at the distance from $-20\lambda_0$ to $-18\lambda_0$ with respect to the center of the incident beam when V_0 varies.

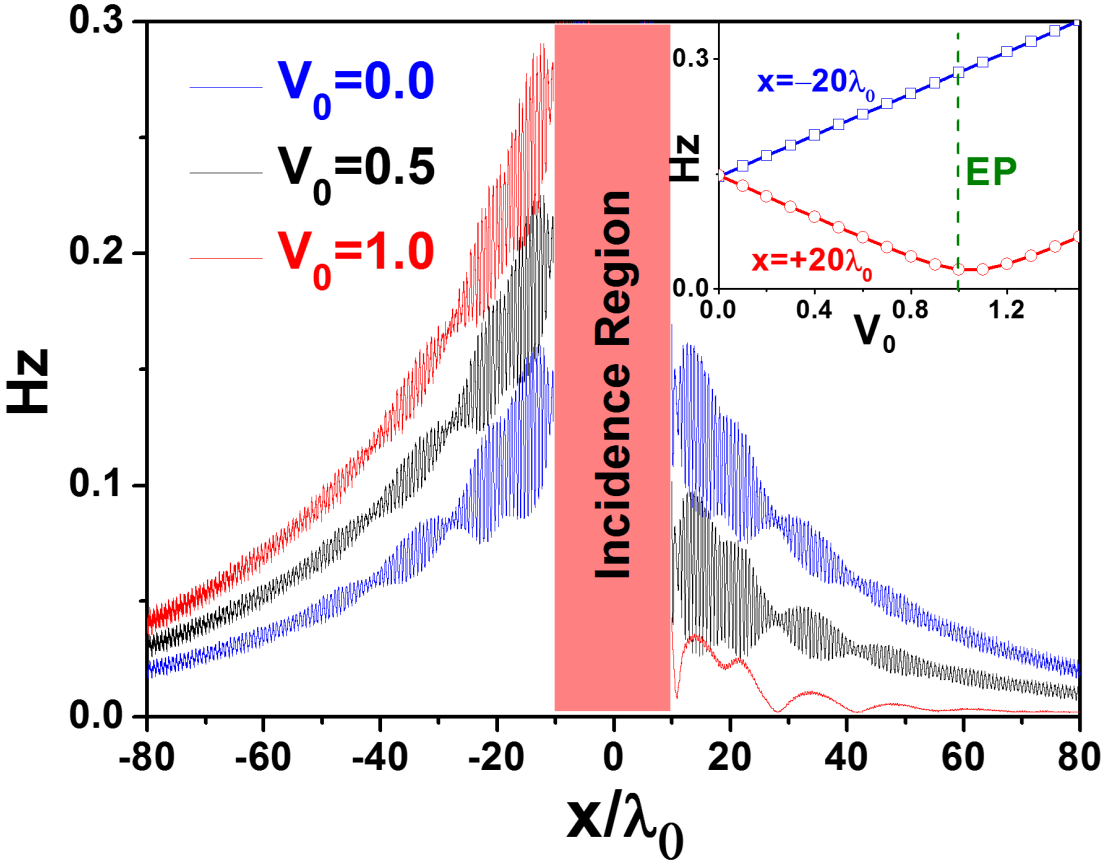

FIG. 3. Distribution of the envelop of H_z at the metal-dielectric interface for V_0=0 (blue line), 0.5 (black line), and 1 (red line), respectively. The field H_z is normalized to the excitation amplitude. The inset shows the variation of field at x= $-20\lambda_0$ and x=$20\lambda_0$ when V_0 varies.

Unidirectional excitation of SPPs has been previously demonstrated via controlling the polarization of illumination [25-27], or using asymmetric nanostructures [28-30]. These results can be well understood from the interference effect of SPPs. In contrast, the underlying mechanism of the unidirectional SPP generation and V_0-dependent excitation efficiency in the *PT* symmetric system is distinctly different, which can be explained by the nonreciprocal nature of the Bloch component through the Fourier analysis of $\varepsilon(x)$. Specifically, the periodical variation of the real and imaginary part of $\varepsilon(x)$ required by the *PT* symmetry can be expressed by using Fourier expansion. A simple expression of the modulation $\Delta\varepsilon(x)=A(\cos\beta x + iV_0\sin\beta x)$ can be obtained as

$$\Delta\varepsilon(x) = A_L\exp(+i\beta x) + A_R\exp(-i\beta x), \quad (3)$$

with

$$A_L = A\frac{1+V_0}{2}, \quad (4)$$

$$A_R = A\frac{1-V_0}{2}. \quad (5)$$

Obviously, the factor $\Delta\varepsilon(x)$ contains two Bloch components $\exp(-i\beta x)$ and $\exp(+i\beta x)$ that represent moving harmonic gratings towards the forward (positive x-axis) and backward (negative x-axis) directions. When V_0 is not zero, A_L and A_R have different values, and this Fourier spectrum is nonreciprocal. On the other hand, the two wavevectors, $+\beta$ and $-\beta$, help to compensate the momentum mismatch between the normally incident wave (with k_x=0) and SPPs (with k_x=$\pm\beta$) according to Bloch's theorem [21, 22]. As a result, we expect to achieve asymmetric excitation of SPPs with the efficiency determined by A_L and A_R, and ultimately by V_0.

The unique characteristics of SPPs in the *PT*-symmetric system can be analyzed by a simple perturbative approach and the coupled mode theory in a general context [36-38]. To include the damping effect, we can modify the Helmholtz equation for the magnetic field component H_z into the form of $\nabla^2 H_z - \frac{\varepsilon_d}{c^2}\left(\frac{\partial^2 H_z}{\partial t^2} + \frac{2}{\tau}\frac{\partial H_z}{\partial t}\right) = \square\frac{\partial^2 H_z}{c^2 \partial t^2}$, where τ represents the relaxation time. Specifically, τ_{abs} is associated with the absorption loss of SPPs due to electron collision, and τ_{rad} is related to the radiative loss. The mutual coupling among the three field components can be described by a non-Hermitian matrix over the complex amplitudes of SPPs (H_L^{SPP} and H_R^{SPP}) and free-space plane wave (H_0) as follows

$$\begin{bmatrix} \omega_0 + i\tau_{abs}^{-1} & A_L V^* M^{-1} & \\ A_R V N^{-1} & \omega_0 + i\tau_{rad}^{-1} & A_L V N^{-1} \\ & A_R V^* M^{-1} & \omega_0 + i\tau_{abs}^{-1} \end{bmatrix} \begin{bmatrix} H_L^{SPP} \\ H_0 \\ H_R^{SPP} \end{bmatrix} = \widetilde{\square} \begin{bmatrix} H_L^{SPP} \\ H_0 \\ H_R^{SPP} \end{bmatrix}. \quad (6)$$

If we use $\square(y)$ to denote the field distribution of the excitation wave inside the *PT*-symmetric dielectric layer, and define $\alpha = \sqrt{\beta^2 - \varepsilon_d k_0^2}$, in Eq. (6) $\mathrm{M} = [1 - \exp(-2\alpha d)]/2\alpha$ and $N = \int_0^d \square(y)\square(y)^* dy$ are the field normalization factors of SPPs and the plane wave, respectively; $V = -\frac{\omega_0}{2\varepsilon_d}\int_0^d \square(y)^* e^{-\alpha y} dy$ characterizes the overlap integral of SPPs and the excitation wave obtained from a perturbative approach [36-38]. The detailed derivation of Eq. (6) can be found in the Supplemental Material.

Being analogue to a coupled three-level configuration in atomic system [39, 40], Eq. (6) usually leads to three complex solutions for frequency $\widetilde{\omega}$ with modified dispersion and decay rate. However, it can be proved (see the Supplemental Material) that regardless the complex solution $\widetilde{\omega}$, the generated SPPs along the forward and backward directions have the identical ratio given by

$$\left|\frac{H_L^{SPP}}{H_R^{SPP}}\right| = \left|\frac{A_L}{A_R}\right|. \quad (7)$$

The weights of A_L and A_R determine the efficiency of SPP excitation. When V_0=0, the two harmonic contributions in $\Delta\varepsilon(x)$ have the identical weight of $A/2$ based on Eqs. (4) and (5). Therefore the generated SPPs have equal amplitudes in the forward and backward directions [see Fig. 2(a)]. In contrast, A_L becomes greater than A_R when V_0 increases, and SPPs are more effectively generated on the left side of incidence.

The most interesting scenario takes place at the critical point of

$$V_0=1, \quad A_R=0. \quad (8)$$

Albeit the excitation of SPPs on the right side of incidence is phase matched, the effective field A_R is zero. Now, because the eigen-solutions coalesce [2-4, 31] an atypical EP emerges, which is not due to a square root singularity. Equation (6) gives only two solutions instead of three. The first solution of the complex frequency and the corresponding field amplitudes are given by

$$\tilde{\omega} = \omega_0 + i\tau_{rad}^{-1}, \quad [H_L^{SPP} \quad H_0 \quad H_R^{SPP}] = [A_L V^* M^{-1} \quad i(\tau_{abs}^{-1} - \tau_{rad}^{-1}) \quad 0], \quad (9)$$

which clearly manifest that SPPs are generated towards the left side only, while the amplitude of the excitation wave is constant. The other solution is

$$\tilde{\omega} = \omega_0 + i\tau_{abs}^{-1}, \quad [H_L^{SPP} \quad H_0 \quad H_R^{SPP}] = [1 \quad 0 \quad 0]. \quad (10)$$

This represents the sole existence of SPPs on the left side, which are not coupled back to either the free-space mode or right-side SPPs, and hence only subjected to the intrinsic absorption loss. Also, the dispersion of SPPs is not modified by the *PT*-symmetric perturbation, although the perturbation allows to excite SPPs.

Equations (8-10) highlight an important feature of an EP in a non-Hermitian system. The scenario of A_R=0 when V_0= 1 (or A_L=0 when V_0= −1) breaks the forth-and-back coupling among the SPP and plane wave components, and closes the possible radiative and absorption loss pathways. Especially, Eq. (10) promises a new route to improve the lifetime (or propagation distance) of the generated SPPs by completely suppressing the backscattering into free-space propagating waves, which can also be explained by an intuitive picture from Bloch's theorem as follows. As we know, the lifetime τ of SPPs contains two contributions, *i.e.*, the absorption loss and radiative loss. The excited SPPs and their radiative loss are associated with the forth-and-back coupling between external incidence and SPPs, mediated by harmonic components with opposite Bloch wavevectors. For example, let us consider the excitation of SPPs to the left side of the incidence, as schematic shown in Fig. 4(a). The efficiency of this scattering process is determined by the factor of $A_L\exp(+i\beta x)$ in $\Delta\varepsilon(x)$. The opposite process, *i.e.*, the backward coupling of SPPs to free-space photons with k_x=0, represents the radiative loss of SPPs. This backward coupling

process requires the harmonic term of $A_R\exp(-i\beta x)$. The efficiencies of these two opposite processes can be substantially different according to Eqs. (4) and (5). Equation (8) represents an extreme scenario of EP, in which

$$\frac{1}{\tau_{rad}^{SPP}} = 0 \tag{11}$$

for the unidirectionally generated SPPs on the left side. This manifests that the backward scattering pathway is completely closed, resulting in the radiative-loss-free effect. Then the loss of SPPs, in theory, is only attributed to the absorption loss. The lifetime of the unidirectionally excited SPPs on the left side of incidence is expected to increase, producing long-range SPPs. Similar conclusions can be made to the forward propagating SPPs when $V_0 = -1$.

We conduct COMSOL simulations to confirm the predicted radiative-loss-free effect. The imaginary part of metal is set to be zero (*i.e.*, $\varepsilon_m = -100$), in order to eliminate the absorption loss and help us to identify the role of backward scattering. Two cases are present here. The first case is similar to that in Fig. 2(c), with A=0.5 and V_0=1, so that A_L=0.5 and A_R=0. The other case is that A=1 and V_0=0, with which A_L=A_R=0.5. The only difference between these two cases is that the first one has a zero backward Bloch component A_R. From the results shown in Fig. 4(b) we indeed observe the radiative-loss-free effect in the first case. Both cases have equal magnitude of SPPs on the left side of incidence. However, when propagating away from the incident beam, SPPs in the first case of V_0=1 (red line) do not decay, while that of V_0=0 (blue line) shows an exponential decay, clearly indicating the presence of radiative loss. Furthermore, when V_0=0 the field possesses a weak oscillation. It is associated with the interference between SPPs and the cascading excited backward surface modes, and implies the existence of an open backward scattering pathway. Such a phenomenon does not arise when V_0=1.

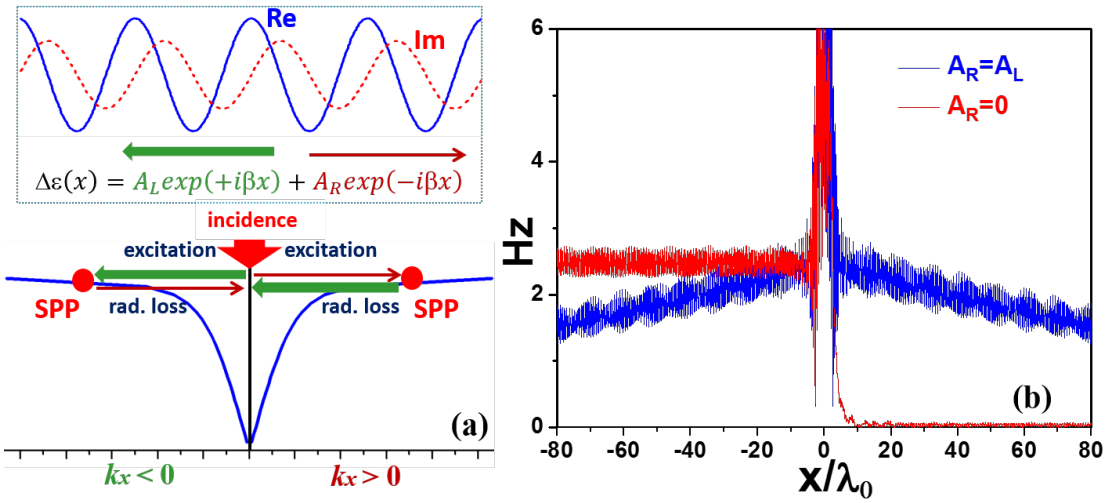

FIG. 4. (a) The excitation of SPPs towards the left and right sides are driven by A_L and A_R, respectively. The backward process of radiative loss is associated with A_R and A_L, accordingly. When A_R=0 the channel of radiative loss on the left side of incidence is closed, (b) Distributions of H_z at A_R=A_L=0.5 (blue line), and A_L=0.5, A_R=0 (red line), respectively. The field when A_R=0 (red line) does not decay due to the radiative-loss-free effect.

Above demonstrated unidirectional radiative-loss-free SPP excitation shows great potential of *PT* symmetry. Unidirectional SPP generation has been investigated by various authors [25-30], for example, via the utilization of vectorial near-field interference [25], interference among multiple elements on the metal surface [26-29], and compact coupled magnetic antennas [30]. Our investigation presented in this Letter is fundamentally different from previous work, because it relies not on the manipulation of localized scattering units, but on the global distribution of refractive index in a geometric flat structure. Furthermore, losses in plasmonic structures and metamaterials have been noticed and believed to be the main obstacle in impeding their practical applications [21-30, 41-49]. One can engineer the shape of nanostructures in order to reduce the fraction of energy confined inside the metal and thus reduce the absorption loss [41-45], or introduce optical gain into the nanostructure to compensate the loss [46-49]. Our approach based on *PT* symmetry provides a new route to eliminate the radiative loss, which can be very strong when sharp edges, scatters, or micro-gratings are present. To the best of our knowledge, the mechanism of closing the backward scattering pathway by utilizing the nonreciprocal Bloch components in *PT* symmetric systems has not been discussed before. The radiative-loss-free feature promises many applications in subwavelength structured optical circuits, for example, generating and routing long-range SPPs for sensing and

communication purposes with high efficiency, low power and fast speed. Although we have focused on the investigation at optical frequencies, the same strategy can be extended to microwave and THz regimes by using spoof SPPs on structured perfect conductors [50, 51]. It is worth pointing out that associated with the radiative-loss-free effect, the dispersion of SPPs is also immune to the *PT*-symmetric perturbation [see Eq. (10)]. This interesting characteristic may facilitate novel plasmonic designs.

In summary, we study the excitation of SPPs at a smooth metal-dielectric interface at normal incidence when the permittivity of the dielectric medium follows *PT* symmetry. It is shown that the loss and gain associated with the imaginary part of the dielectric constant can be engineered to realize unidirectional SPP excitation. We explain this novel effect by emphasizing that the *PT* symmetry produces different weights on the Bloch expansion terms with opposite wavevctors $k= \pm\beta$. Such a unique property can also facilitate to suppress and even eliminate the backward scattering from SPPs into free-propagating light waves, rendering a radiative-loss-free effect at an EP senario. Full-wave simulations confirm our analytical predictions. Our results show that *PT* symmetry can find many potential applications in nanoscale optical devices, such as plasmonic routers and isolators for optical computation, communication and information processing.

Acknowledgment

We appreciate Prof. Li Ge for the very helpful discussions during the revision process of the work. Y. M. L. acknowledges the partial financial support from the Office of Naval Research under award number N00014-16-1-2409. J. C. acknowledges the support from the National Natural Science Foundation of China (NSFC) under grants 11574162. W. W., L. Q. W., and R. D. X. acknowledge the Innovative Research Fund for 100 undergraduates of Nankai University under grants BX14130, BX14124, and BX14137.

W. W., L. Q. W., and R. D. X. contribute equally to this work.

References

1. C. M. Bender and S. Boettcher, Phys. Rev. Lett. **80**, 5243 (1998).
2. W. D. Heiss, Phys. Rev. E **61**, 929 (2000).
3. N. Moiseyev, *Non-Hermitian quantum mechanics* (Cambridge University Press, London, 2011).
4. H. Cao and J. Wiersig, Rev. Mod. Phys. **87**, 61 (2015).
5. K. G. Makris, R. El-Ganainy, D. N. Christodoulides, and Z. H. Musslimani, Phys.

Rev. Lett. **100**, 103904 (2008).
6. A. Guo, G. J. Salamo, D. Duchesne, R. Morandotti, M. Volatier-Ravat, V. Aimez, G. A. Siviloglou, and D. N. Christodoulides, Phys. Rev. Lett. **103**, 093902 (2009).
7. E. Ruter, K. G. Makris, R. El-Ganainy, D. N. Christodoulides, M. Segev, and D. Kip, Nat. Phys. **6**, 192 (2010).
8. S. Longhi, Phys. Rev. A **82**, 031801 (2010).
9. Y. D. Chong, L. Ge, and A. D. Stone, Phys. Rev. Lett. **106**, 093902 (2011).
10. Z. Lin, H. Ramezani, T. Eichelkraut, T. Kottos, H. Cao, and D. N. Christodoulides, Phys. Rev. Lett. **106**, 213901 (2011).
11. L. Feng, Y. L. Xu, W. S. Fegadolli, M. H. Lu, J. E. B. Oliveira, V. R. Almeida, Y. F. Chen, and A. Scherer, Nat. Mat. **12**, 108 (2013).
12. Regensburger, C. Bersch, M. Mohammad-Ali, G. Onishchukov, D. N. Christodoulides, and U. Peschel, Nature **488**, 167 (2012).
13. L. Ge, Y. D. Chong, and A. D. Stone, Phys. Rev. A 85, 023802 (2012).
14. R. Fleury, D. L. Sounas, and A. Alu, Phys. Rev. Lett. **113**, 023903 (2014).
15. B. Peng, S. K. Ozdemir, S. Rotter, H. Yilmaz, M. Liertzer, F. Monifi, C. M. Bender, F. Nori, and L. Yang, Science **346**, 328 (2014).
16. M. Lawrence, N. Xu, X. Zhang, L. Cong, J. Han, W. Zhang, and S. Zhang, Phys. Rev. Lett. **113**, 093901(2014).
17. K. V Kepesidis, T. J. Milburn, J. Huber, K. G. Makris, S. Rotter, and P. Rabl, New J. Phys. **18,** 095003 (2016).
18. L. Ge and H. E. Türeci, Phys. Rev. A 88, 053810 (2013).
19. M. Kang, F. Liu, and J. Li, Phys. Rev. A 87, 053824 (2013).
20. V. V. Konotop, J. Yang, and D. A. Zezyulin, Rev. Mod. Phys. **88,** 035002 (2016).
21. V. Zayatsa, I. I. Smolyaninovb, and A. A. Maradudin, Physics Reports **408**, 131 (2005).
22. F. J. Garcia-Vidal, L. Martin-Moreno, T. W. Ebbesen, and L. Kuipers, Rev. Mod. Phys. **82**, 729 (2010).
23. Y. M. Liu and X. Zhang, Chemical Society Reviews **40**, 2494 (2011).
24. J. B. Khurgin, Nature Nano. **10**, 2 (2015).
25. F. J. Rodriguez-Fortuno, G. Marino, P. Ginzburg, D. O'Connor, A. Martinez, G. A. Wurtz, A. V. Zayats, Science **340**, 328 (2013)
26. J. Lin, J. B. Mueller, Q. Wang, G. Yuan, N. Antoniou, X. C. Yuan, F. Capasso, Science **340**, 331 (2013).
27. L. Huang, X. Chen, B. Bai, Q. Tan, G. Jin, T. Zentgraf, and S. Zhang, Light: Science & Applications **2**, e70 (2013).

28. F. López-Tejeira, S. G. Rodrigo, L. Martín-Moreno, F. J. García-Vidal, E. Devaux, T. W. Ebbesen, J. R. Krenn, I. P. Radko, S. I. Bozhevolnyi, M. U. González, J. C. Weeber, and A. Dereux, Nat. Phys. **3**, 324 (2007).
29. J. S. Q. Liu, R. A. Pala, F. Afshinmanesh, W. Cai, and M. L. Brongersma, Nat. Commun. **2**, 525 (2011).
30. Y. Liu, S. Palomba, Y. Park, T. Zentgraf, X. Yin, and X. Zhang, Nano Letters **12**, 4853 (2012).
31. X. B. Yin and X. Zhang, Nat. Mater. **12**, 175 (2013).
32. K. G. Makris, R. El-Ganainy, D. N. Christodoulides, and Z. H. Musslimani, Phys. Rev. A **81**, 063807 (2010).
33. F. J. Shu, C. L. Zou, X. B. Zou, and L. Yang, Phys. Rev. A **94**, 013848 (2016).
34. Comparable parameter can be obtained, for example, in Silver around 1.3 μm. See M. N. Polyanskiy. "Refractive index database," http://refractiveindex.info (accessed Dec. 6 2016)
35. Y. Liu, T. Zentgraf, G. Bartal, and X. Zhang, Nano Lett. **10**, 1991 (2010).
36. D. Marcuse, Bell Labs Technical Journal 48, 3187 (1969).
37. D. Marcuse, Theory of dielectric optical waveguides (New York, Academic Press 2013).
38. J. B. Khurgin and Y. J. Ding, Optics letters 19, 1016 (1994).
39. M. O. Scully and M. S. Zubairy, *Quantum Optics* (Cambridge University Press, London, 1997).
40. S. Longhi, Laser and Photon. Rev. **3** 243 (2009).
41. J. B. Khurgin and A. Boltasseva, MRS BULLETIN **37**, 768 (2012).
42. S. A. Maier and H. A. Atwater, J. Appl. Phys. **98**, 011101 (2005).
43. S. I. Bozhevolnyi, V. S. Volkov, E. Devaux, and T. W. Ebbesen, Phys. Rev. Lett. **95**, 046802 (2005).
44. J. A. Dionne, L. A. Sweatlock, and H. A. Atwater, Phys. Rev. B **73**, 035407 (2006).
45. P. Berini, Adv. Opt. Photo. **1**, 484 (2009).
46. D. J. Bergman and M. I. Stockman, Phys. Rev. Lett. **90**, 027402 (2003).
47. M. I. Stockman, Nat. Photonics **2**, 327 (2008).
48. M. A. Noginov, G. Zhu, A. M. Belgrave, R. Bakker, V. M. Shalaev, E. E. Narimanov, S. Stout, E. Herz, T. Suteewong, and U. Wiesner, Nature **460**, 1110 (2009).
49. R. F. Oulton, V. J. Sorger, T. Zentgraf, R. M. Ma, C. Gladden, L. Dai, G. Bartal, and X. Zhang, Nature **461**, 629 (2009).
50. J. B. Pendry, L. Martin-Moreno, and F. J. Garcia-Vidal, Science **305**, 847 (2004)

51. A. P. Hibbins, B. R. Evans, J. R. Sambles, Science **308**, 670 (2005)